A NEURAL NETWORK APPROACH FOR VOLCANIC MONITORING OF SULPHUR DIOXIDE USING HYPERSPECTRAL REMOTE SENSED DATA

Alessandro Piscini [1], Elisa Carboni[2], Roy Don Granger [2], Fabio Del Frate[3]

[1] *Istituto Nazionale di Geofisica e Vulcanologia, Via di Vigna Murata 605 Roma, Italy EMail: alessandro.piscini@ingv.it:*

[2] *AOPP, Physics Department, University of Oxford, Clarendon Laboratory, Parks Road, OX1 3PU Oxford, UK, E-mail: elisa@atm.ox.ac.uk, r.grainger@physics.ox.ac.uk*

[3] *Earth Observation Laboratory, Engineering department Tor Vergata University, Via del Politecnico 1, 00133, Rome, Italy, E-mail: delfrate@disp.uniroma2.it.*

ABSTRACT

This paper describes an application of ANN for the simultaneous estimation of the columnar content and height of the SO_2 plume from volcanic eruptions using hyperspectral remotely sensing data. ANN have been trained using all IASI channels between 1000–1200 and 1300–1410 cm^{-1}, as inputs, and the corresponding values of SO_2 amount and plume's height obtained using the Oxford retrieval scheme as outputs. As a case study we have chosen the Eyjafjallajökull volcano (Iceland), in particular the eruption took place during the months of April and May 2010, which had an enormous impact on the world economy. ANNs have been validated on some independent data sets belonging to the same eruption and also on IASI images of Grímsvötn eruption, occurred on May 2011. The results have provided values of RMSE between ANN outputs and targets always less than 20 DU for SO_2 and 200 mb for height, so demonstrating the good performance in retrieval achieved by the ANN technique.

1. INTRODUCTION

The eruption of the Eyjafjallajökull volcano, which took place in Iceland in April and May 2010, revealed the importance of the effects produced by such a natural event for human safety [1] and showed the importance of having reliable real-time monitoring in place for volcanic ash and sulphur dioxide, especially in the aviation sector [2]. Volcanic ash plumes from the eruption of Eyjafjallajökull in April 2010 resulted in the cancellation of 107,000 flights in Europe (or 48% of total traffic) affecting about 10 million passengers.

Satellite remote sensing is an invaluable tool for monitoring volcanic events on a large scale and in a short time because such natural disasters may have effects on the population and the economy of affected areas.

Estimating SO_2 is a very important task because of the critical role that its plume plays as a proxy for volcanic ash, especially within a few hours after release when the effects of wind shear and of gravitation have not yet divided the ash plume from the SO_2.

For these reasons, accurate and readily available data are needed to properly monitor the evolution of the phenomena and to manage the risk mitigation phase.

Quantitative estimation of SO_2 is usually obtained by applying algorithms based on a comparison between top of atmosphere (TOA) radiance and values obtained from simulations run using a radiative transfer model: this requires long computation times and many parameters as input [3] [4].

More recent estimates of columnar content of SO2 in the atmosphere as a result of volcanic eruptions are available using hyperspectral data from various sensors operating in different spectral ranges from UV to IR, e.g. Ozone Monitoring Instrument (OMI) [5], Global Ozone Monitoring Experiment 2 (GOME-2) [6], Atmospheric Infrared Sounder (AIRS) [7], Infrared Atmospheric Sounding Interferometer (IASI) [8] [9] [10].

IASI is the only infrared spectrometer with global coverage every 12 hours (METOP A), and now that METOP B is available there should be no coverage gaps. Its spectral resolution is slightly higher than AIRS, and its spectrum includes both absorption bands of SO2 at 8.7 and 7.3 μm (AIRS only senses the 7.3 μm band). Another IR spectrometer with an even higher spectral resolution is Tropospheric Emission Spectrometer (TES), but it has very limited coverage (narrow swath).

Artificial neural networks (ANN), computational modelling tools, have found wide acceptance in many disciplines due to their adaptability to complex real world problems.

ANNs have demonstrated their ability to model non-linear physics systems [11] involving complex physical behaviours, and were applied to the analysis of remotely sensed images with promising results. Some examples are: retrieval of soil moisture and agricultural variables from microwave radiometry [12], snow water equivalent and snow water depth from microwave images [13], retrieval of leaf area index (LAI) and other

Proc. 'ESA Living Planet Symposium 2013', Edinburgh, UK
9–13 September 2013 (ESA SP-722, December 2013)

biophysical variables from the MERIS and MODIS instruments [14] [15], estimation of chlorophyll from MERIS [16].
Recently, ANNs have been applied to MODIS multispectral measurements to retrieve volcanic ash parameters such as effective radius and aerosol optical depth [17], and NNs have also been used operationally to estimate CO, CO2 and CH4 column amounts from IASI [18]. The current study represents a first attempt at applying ANN to hyperspectral remote sensing data, for simultaneous estimates SO_2 total columnar content and plume height. The present work, compared to recent results of ANN usage with multispectral data, shows significant added value in reduced execution times during ANN application stage. Another result of this approach is the simultaneous estimation of both columnar content of SO_2 and plume height from high spectral resolution data provided by the IASI spectrometer on board the satellite Meteorological Operational satellite program (METOP) since 2006.

2. METOP-IASI IASI Sensor

The IASI sensor is aboard METOP, a European weather satellite which has been operating since 2007. METOP is the first of three satellites scheduled to operate for fourteen years. It crosses the Equator on the descending node at a local time of 9.30. IASI is a Fourier transform spectrometer which covers the spectral range 645-2760 cm^{-1} (3.62 to 15.5 μm) with spectral sampling of 0.25 cm^{-1} and spectral resolution of 0.5 apodized cm^{-1} [19]. It has a nominal radiometric accuracy of 0.25–0.58 K. The field-of-view (FOV) consists of four circular footprints of 12 km diameter (at nadir) inside a square of 50 × 50 km, step-scanned across tracks (30 steps). It has a 2000 km wide swath and nominally it can achieve global coverage in 12 h. IASI carries out nadir observation of the earth simultaneously with Global Ozone Monitoring Experiment (GOME-2) also onboard METOP. GOME-2 is a UV spectrometer measuring SO_2 in the UV absorption band and was used for both Differential Optical Absorption Spectroscopy (DOAS) [6] and optimal estimation retrievals (Nowlan et al., 2011) of SO_2; more information on IASI can be found in [20].
IASI level 1c data (geolocated and apodized spectra) used here were obtained from both the British Atmospheric Data Center (BADC) archive and EUMETSAT Unified Meteorological Archive Facility (UMARF) archive.

3. SO_2 RETRIEVAL DESCRIPTION

The SO_2 column amount and altitude reference values were generated using an optimal estimation scheme applied to IASI measurements of the ν3 and ν1 absorption bands, centred at about 8.7 and 7.3 μm, respectively [10]. This retrieval technique uses a new approach to compute and use an error covariance matrix, Se, based on an SO_2-free climatology of differences between the IASI and forward modelled spectra. Any differences not related to SO_2 between IASI spectra and those simulated by a forward model are included in the covariance matrix, allowing a comprehensive error budget to be computed for every pixel.
As IASI measures atmospheric emission, it provides continuous measurements throughout an orbit. The IASI retrieval follows the method of [10] where SO_2 concentration is modelled by a Gaussian profile. The optimal estimation technique of [21] is then used to estimate SO_2 column amount and the height of the SO_2 profile, and the surface skin temperature using IASI measurements from 1000 to 1200 cm^{-1} and from 1300 to 1410 cm^{-1} (the ν1 and ν3 SO_2 bands).
The forward model is based on RTTOV [22] extended to include SO_2 explicitly, and uses ECMWF profiles of temperatures and water vapor interpolated to IASI measurement time and location. The ECMWF dataset used is the operational one: http://www.badc.rl.ac.uk/data/ecmwf-op/.
Note that: (i) in addition to the SO_2 column amount retrievals return an estimate of the plume altitude (under the assumption that vertical concentrations of SO_2 follow a Gaussian distribution), when the column amount is > ~2 DU and the plume height represents the altitude where the Gaussian profile reaches a maximum; (iii) SO_2 retrieval is not affected by underlying clouds (if SO_2 is within or below an ash or cloud layer its signal will be masked and retrieval will underestimate the SO_2 amount; in the case of ash this is indicated by a cost function value greater than two); (iii) an error covariance matrix is provided per pixel.
The total mass of SO_2 in the atmospheric plume is obtained by interpolating the accepted data into a 0.125° grid and this is presented in Fig. 1. Error bars shown are the worst scenario of correlated error, obtained as a sum of all pixel errors (an overestimate, compared to independent errors). Fig. 1 shows the values of total mass obtained considering all the plume pixels (with latitude between 30° and 80° N and longitude between −50° and 40° E), taking into account only the pixels complying with quality control criteria (convergence and cost function lower than two). Results show that the Oxford SO_2 retrieval scheme for IASI follows the different phases of a medium intensity eruption in the lower troposphere such as Eyjafjallajökull, in some phases consistent with GOME-2, OMI, even if estimates from different satellites can vary significantly.

4. NEURAL NETWORK METHODOLOGY

Artificial Neural Networks (ANN) are based on the concept of the single artificial neuron, the 'Perceptron', introduced by Rosenblatt in 1958 [23] to solve problems

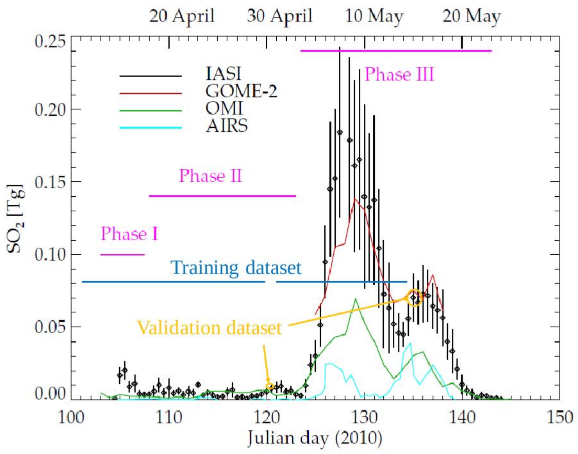

Figure 1. Estimate of total mass of SO_2 present in the Eyjafjallajökull plume from Carboni et al. (2012): IASI data (and error bars) are shown in black, GOME-2 values (Rix et al., 2012) are shown in red, OMI values (Thomas and Prata, 2011) are shown in green, AIRS values (Thomas and Prata, 2011) are shown in cyan. Training and validation datasets used in this paper are here indicated with dark blue and yellow.

in the area of character recognition [24]. An artificial processing neuron receives inputs as stimuli from the environment, combines them in a special way to form a 'net' input that is sent through a linear threshold gate, and transmits the output signal forward to another neuron or the environment. Only when the 'net input' exceeds the threshold limit of a neuron (also called bias), does the neuron become activated. The activation of a given node is calculated using a transfer function (e.g. sigmoidal function) to yield an output between 0 and 1 or -1 and +1. The amount of activation obtained represents a new signal, transferred forward to a subsequent layer (e.g. either hidden or output layer). The same procedure of calculating the net effect is repeated for each hidden node and for all hidden layers [25]. Perceptrons can be trained on a set of examples using a special learning rule [24], and the perceptron weights (including the threshold) are changed in proportion to the difference (error) between the target (correct) output, and their solution, for each example.

Error is a function of all the weights and it forms an irregular multidimensional complex hyper plane with many peaks, saddle points, and minima. Using a specialized search technique, the learning process yields the set of weights corresponding to a global minimum. One of them is the Backpropagation algorithm (BP), which consists of two phases: in the feedforward pass, an input vector is presented to the network and propagated forward to the output; in the backpropagation phase, the network output is compared to a desired output; network weights are then adjusted in accordance with an error-correction rule [26], [25] or [27].

The performance of a trained ANN is generally assessed by computing the root mean squared error (RMSE) between expected values and activation values at the output nodes or, in the case of classification, a percentage of correctly classified examples of the validation set.

In order to cope with non linearly discrete problems, additional layer(s) of neurons placed between the input layer (containing input nodes) and the output neuron are needed, leading to the Multilayer Perceptron (MLP) architecture [24].

In this work Backpropagation Neural Network (BPNN) was used.

A BPNN is an MLP consisting of an input layer with nodes representing input variables to the problem, an output layer with nodes representing the dependent variables (i.e. what is being modelled), and one or more hidden layers containing nodes to help capture nonlinearities in the data. Using supervised learning, with the Error-Correction Learning (ECL) rule for network weights adjustment, those networks can learn to map from one data space to another using examples. The term back-propagation refers to the way the error computed at the output side is propagated backwards from the output layer to the hidden layer, and finally to the input layer. In BPNNs, data are fed forward into the network without feedback (i.e. all links are unidirectional and there are no same layer neuron-to-neuron connections). The neurons in BPNNs can be fully or partially interconnected. Networks like this are versatile and can be used for data modelling, classification, forecasting, control, data and image compression, as well as pattern recognition [28].

A neural network for SO_2 total column estimation and another for SO_2 plume height estimation were implemented using, as training sets, SO_2 column content values and SO_2 plume height values from IASI optimal estimation retrieval [10], computed processing brightness temperatures from 58 IASI images. Data were acquired from both morning and afternoon orbits in the period 14 April to 15 May 2010. Both networks used acquired Brightness Temperature data as neural network inputs and SO_2 total column and plume height as target output respectively. Sample patterns statistics encompassed the entire duration of the Eyjafjallajökull eruption and they were considered a good training ensemble, because data covered all three eruptive phases. Spatial and statistical distributions of training sets for SO_2 columnar content and plume height are shown in Fig. 2, top-left and top-right. Network topologies, both for SO_2 total column content and plume height neural network, consisted of 1242 inputs, all IASI channels, representing the range of wavelengths which contain information on SO_2 and used in the IASI retrieval, ten neurons in one hidden layer and one

output.
Cross validation can be used to detect when over-fitting starts during supervised training of a neural network; training is then stopped before convergence to avoid over-fitting (early stopping). Early stopping using cross validation was done by splitting the training data into a training set, a validation set, and a test set, and then training the networks only using the training set and evaluating the per-example error on the test set on a sample basis after a defined number of epochs. Finally, training was stopped when the error, the difference between neural network output and target (retrievals from [10], on the cross validation set was higher than the previous error value [29].

5. RESULTS AND DISCUSSION

In order to evaluate the performance of neural networks in terms of retrieval accuracy and generalization capability, both neural networks for SO_2 total column content and plume height estimation were applied to three distinct independent IASI images related to the Eyjafjallajökull eruption (see section 4.1), and to three independent datasets related to another Iceland volcanic eruption (from Grímsvötn, which occurred during May 2011). Regarding the Eyjafjallajökull validation datasets, two images used were from morning and afternoon orbits of the same day (15 May 2010) in order to verify neural network performance on both illumination conditions, the third image (30 April) has been chosen in order to test the NN performance with low SO_2 amount. Fig. 2 shows the spatial distribution of the total mass of SO_2 for the Eyjafjallajökull training and validation datasets.

Table 1. RMSE values related to Sulphur Dioxide total column estimated by the NN for independent Eyjafjallajökull validation sets, STD and mean difference percentage

Date	SO_2 total column [DU]				
	samples	Regr. Coeff.	RMSE	STD	Mean diff. %
2010/04/30 aft	161	0.9523	0.7577	1.8084	16.9529
2010/05/15 mor	1823	0.93008	1.0523	2.7471	4.3728
2010/05/15 aft	2303	0.94372	0.8722	2.1335	8.7850

For sulphur dioxide total columnar content, RMSE is, for all three datasets, lower than the corresponding values of the targets' standard deviation (STD), which can be seen as an indication of distribution spreading and measurement mean value error bar widening. In

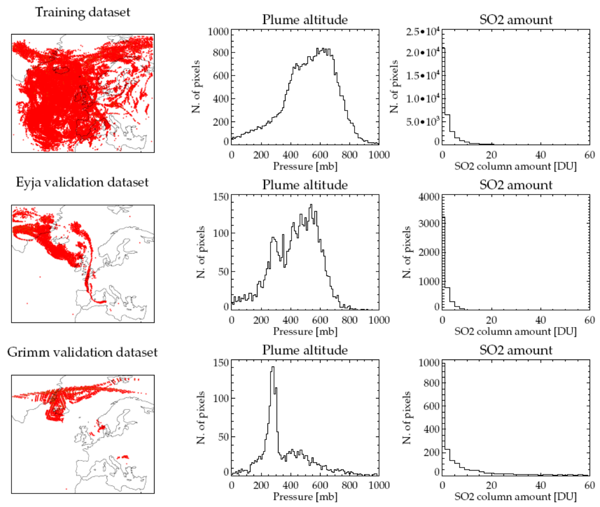

Figure 2. Spatial distribution maps of IASI Sulphur dioxide (left), divided into training set (top), Eyjafjallajökull validation dataset (middle), Grímsvötn validation dataset (bottom) and Sulphur dioxide plume height and total column content statistical distribution for each dataset represented by histograms (middle and right)

Table 2. RMSE values related to Sulphur Dioxide plume height estimated by the NN for independent Eyjafjallajökull validation sets, STD and mean difference percentage

Date	SO_2 plume height [mb]				
	samples	Regr. Coeff.	RMSE	STD	Mean diff. %
2010/04/30 aft	161	0.84749	83.1373	124.543	3.4880
2010/05/15 mor	1823	0.84314	87.6765	150.815	-0.4420
2010/05/15 aft	2303	0.83194	71.2645	153.273	-1.1068

particular, looking at Tab. 1, we can see that the 30 April validation shows the lowest RMSE value and the highest regression coefficient.
An interesting behaviour of the NN is seen in the May results. The regression coefficient is always around 0.9 (0.93 for morning orbit and 0.94 for afternoon orbit) but looking at the regression curves depicted in Fig. 3, for 15 of May, morning orbit (top-right), there is a noticeable decrease of performance for target values higher than 10 DU.
We hypothesised that the better performance of the NN in April is due to a lower number of samples (one order of magnitude with respect to the other two dates) and a range of values always below 10 DU, which represent most of the training sample values, instead values higher than 10 DU represent only 6% of training data. Nevertheless, considering the difference percentage of estimate and target means (Tab. 1, last column) the

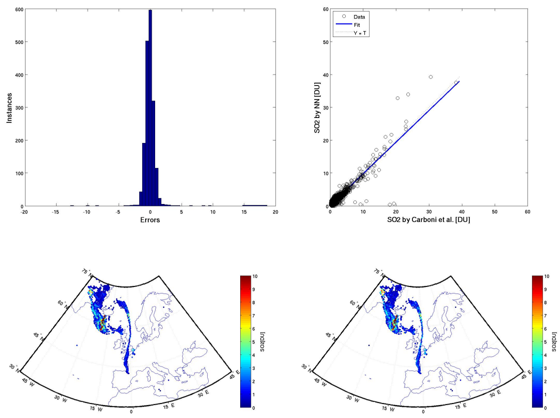

Figure 3. Eyjafjallajökull validation dataset, 15 May 2010, morning orbit. Top - Error distribution (left) and regression curve (right) for neural networks of SO2 total column estimation. Y and T in legend represent estimated values and target values, respectively. Bottom - SO2 total column map from retrieval (left) and Neural Network (right).

April results show an overestimate of retrievals with higher percentage.

The good performance of the NN for sulphur dioxide retrieving is confirmed by Fig. 3 (bottom) representing the comparison of the NN retrieval map with those from [10].

Statistical results of applying of neural network to plume height estimation are summarized in Tab. 2. It is noticeable that for all three datasets RMSE is always below the corresponding values of the targets' standard deviation (STD).

In particular, April 30 shows a lower error dispersion (Fig. 3, bottom-left) and a lower regression coefficient than May 15.

In general, the error spread in plume height is higher than that obtained for the sulphur dioxide total column retrieval. This is confirmed by the regression coefficient obtained and corresponding RMSE. Nevertheless, the NN estimates show good accuracy with RMSE values lower than corresponding STD for all dates and the percentage difference between the estimate and target means are very low. The regression curves for May 15, depicted in Figures 4 (top-rgiht), show a good performance of the retrieval in the range 500-700mb (5000-3000 m).

The validation on the Grimsvotn eruption occurring during May 2011, was centred on three distinct IASI images on the 22, 23 and 24 May 2011. These images were not considered during the NNs training phase.

For SO_2 total column retrieval, looking at Tab. 3 a first generalization can be done since a lower accuracy inretrieval is noticeable for all three validation dates and,

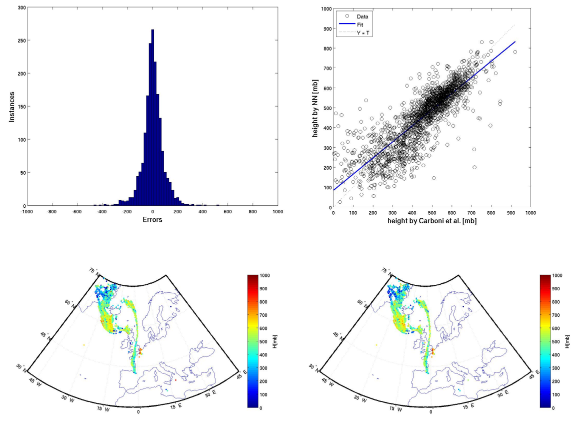

Figure 4. Eyjafjallajökull validation dataset, 15 May 2010, morning orbit. Top - Error distribution (left) and regression curve (right) for neural networks of SO2 plume height estimation. Y and T in legend represent estimated values and target values, respectively. Bottom - SO2 plume height map from retrieval (left) and Neural Network (right).

Table 3. RMSE values related to Sulphur Dioxide total column estimated by the NN for independent Grímsvötn validation sets, STD and mean difference percentage

Date	SO_2 total column [DU]				
	samples	Regr. Coeff.	RMSE	STD	Mean diff. %
22 May 2011	293	0.92719	15.858	31.3802	-25.7537
23 May 2011	678	0.92411	10.558	22.4618	-19.2664
24 May 2011	584	0.93933	1.1593	3.3554	-7.0970

Table 4. RMSE values related to Sulphur Dioxide plume height estimated by the NN for independent Grímsvötn validation sets, STD and mean difference percentage

Date	SO_2 plume height [mb]				
	samples	Regr. Coeff.	RMSE	STD	Mean diff. %
22 May 2011	293	0.71933	141.751	178.369	7.1257
23 May 2011	678	0.78345	118.220	177.977	4.2754
24 May 2011	584	0.77707	109.119	166.896	4.3897

despite regression coefficients are similar to those of the Eyjafjallajökull validations, RMSE and mean difference percentage values are higher. In particular, negative values of this last index reveal that the NN underestimates sulphur dioxide retrieval in all three cases.

The lower accuracy observed can be analysed more in detail with the scatter-plots and maps depicted in Fig. 5. The behaviour is noticeable for the 23 May 2011 estimates in the scatter-plot of Figure 5 (top-right). It shows a decreasing of accuracy for sulphur dioxide values higher than 10 DU and mean value difference percentage around -20%, confirming an underestimation again. If we have a look at Fig. 5 (bottom), the map comparison between target and estimates, we notice the underestimation characterizes pixels on a strip along the 75° N parallel.
A distinct performance is noticed when the NN is applied to 24 May. RMSE is of the order of magnitude of those observed for the Eyjafjallajökull eruption, and also the mean difference percentage is comparable to 2010.

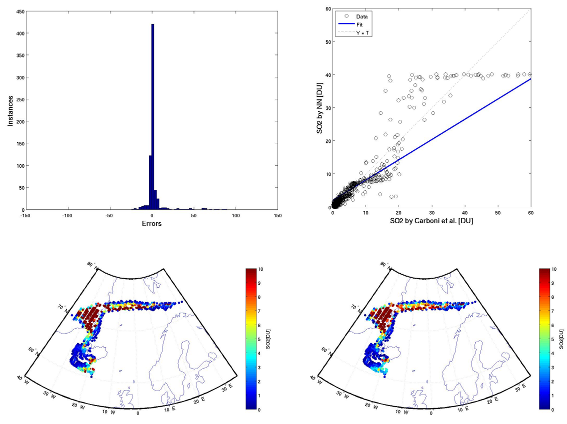

Figure 5. Grimsvotn validation dataset, 23 May 2011, 10:00 UTC. Top - Error distribution (left) and regression curve (right) for neural networks of SO_2 total column estimation. Y and T in legend represent estimated values and target values, respectively. Bottom - SO_2 total column map from retrieval (left) and Neural Network (right).

This distinct behaviour of performances can be explained by considering that, with the exception of 24 May 2011, the mean value of samples for 2011 are around an order of magnitude greater than those of 2010 Eyjafjallajökull instances, for both training and validation dates. In other words Grimsvotn eruption was characterized by sulphur dioxide concentrations higher than those used during NN training phase demonstrating how NNs performance decrease when try to estimates parameters characterized by values outside that of training set.
As regards applying the NN to Grimsvotn dates for height plume retrieval, Tab. 4 summarizes the results for all three.
The 22 May shows the lowest regression coefficient, the highest RMSE and a slightly higher percentage of retrieval overestimation, visible in Fig. 12 (top) for those pixels (green) located in the north of Iceland around 70°N.
The 23 and 24 May test cases reveal a slight increase in coefficient regression, around 0.8, and lower values of RMSE (Tab. 4), and in scatter-plots depicted in Figs. 10 and 11 (bottom-right), respectively, show the NN plume height retrieval is overestimated. In particular, for 23 May, Figure 6 (bottom) shows overestimation over Greenland, around 70°N, whilst, for 24 May overestimation is located in the south, close to Norway. In general, looking at the dispersion error histograms depicted in Fig. 6 (bottom, left) it seems that for plume height estimation the NN reveal a lower performance when applied to unknown eruptions with different characteristics in terms of sulphur dioxide

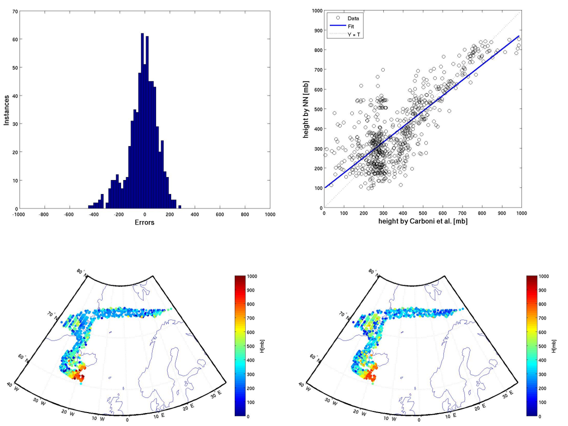

Figure 6. Grimsvotn validation dataset, 23 May 2011, 10:00 UTC. Top - Error distribution (left) and regression curve (right) for neural networks of SO_2 plume height estimation. Y and T in legend represent estimated values and target values, respectively. Bottom - SO_2 total column map from retrieval (left) and Neural Network (right).

concentrations, plume height and spatial distribution.

6. CONCLUSIONS

The analysis demonstrates that Artificial Neural Network is able to retrieve both SO_2 column abundance and plume height with good accuracy if applied to a known eruption and also taking into account that the goal was to replicate a model and no real measurements have been used. Nevertheless the results obtained, applying the NN to an eruption not known, such as the Grimsvotn one, show that great care has to be taken during the training phase. This is because the Neural Network retriever needs to be fed and trained continuously during its operating phase in order to maintain phenomena knowledge updated and retrieval's performance accurate at operating stage.

7. REFERENCES

1. Zehner, C., ed. (2010). Monitoring Volcanic Ash from Space. In: Proceedings of the ESA-EUMETSAT workshop on the 14 April to 23 May 2010 eruption at the Eyjafjoll volcano, South Iceland, Frascati, Italy, 26–27 May 2010, ESA-Publication STM-280. doi:10.5270/atmch- 10-01.

2. Miller, T.P., and Casadevall, T.J. (2000). *Volcanic ash hazards to aviation. In Sigurdsson, H., ed., Encyclopedia of Volcanoes*, San Diego, Academic Press, 915-930.

3. Berk, A., Bernstein, L.S., Robertson, D.C. (1989). MODTRAN: A Moderate Resolution Model for LOWTRAN 7.

4. Anderson, G. P., Wang, J., and Chetwynd, J. H. (1995). MODTRAN3: An update and recent validation against airborne high resolution interferometer measurements. In Summaries of the Fifth Annual Jet Propulsion Laboratory Airborne Earth Science Workshop, **95**–1(1), 5–8.

5. Krotkov, N. A., Carn, S. A., Krueger, A. J., Bhartia, P. K., and Yang, K. (2006). Band residual difference algorithm for retrieval of SO2 from the Aura Ozone Monitoring Instrument (OMI), *IEEE Trans. Geosci. Remote Sens.*, **44**, 1259–1266.

6. Rix, M., Valks, P., Hao, N., Loyola, D. G., Schlager, H., Huntrieser, H. H., Flemming, J., Koehler, U., Schumann, U., and Inness, A. (2012). Volcanic SO2, BrO and plume height estimations using GOME-2 satellite measurements during the eruption of Eyjafjallajökull in May 2010, *J. Geophys. Res.*, **117**, D00U19, doi:10.1029/2011JD016718.

7. Prata, A.J., Bernardo, C., (2007). Retrieval of volcanic SO2 column abundance from Atmospheric Infrared Sounder data, *JJ. Geophys. Res.*, **112**, D20204.

8. Clarisse, L., Coheur, P. F., Prata, A. J., Hurtmans, D., Razavi, A., Phulpin, T., Hadji-Lazaro, J., and Clerbaux, C. (2008). Tracking and quantifying volcanic SO2 with IASI, the September 2007 eruption at Jebel at Tair, *Atmos.. Chem. Phys*, **8**, 7723–7734, doi:10.5194/acp-8-7723-2008.

9. Walker, J. C., Carboni, E., Dudhia, A., and Grainger, R. G. (2012). Improved detection of sulphur dioxide in volcanic plumes using satellite-based hyperspectral infra-red measurements: application to the Eyjafjallajökull 2010 eruption, *J. Geophys. Res.*, **117**, D00U16, doi:10.1029/2011JD016810.

10. Carboni, E., Grainger, R., Walker, J., Dudhia, A., and Siddans, R. (2012). A new scheme for sulphur dioxide retrieval from IASI measurements: application to the Eyjafjallajökull eruption of April and May 2010, *Atmos. Chem. .Phys*, **12**, 11417-11434, doi:10.5194/acp-12-11417-2012.

11. Rumelhart, D.E., Durbin, R., Golden, R., Chauvin, Y. (1995). Backpropagation: the basic theory. In: Rumelhart, D.E., Yves, C. (Eds.), Backpropagation: Theory, Architecture, and Applications. Lawrence Erlbaum, NJ, 1–34.

12. Del Frate, F., Ferrazzoli, P., Schiavon, G. (2003). Retrieving soil moisture and agricultural variables by microwave radiometry using neural networks, *Remote Sens. Environ.*, **84**(2), 174-183.

13. Tedesco, M., Pulliainen, J., Takala, M., Hallikainen, M., Pampaloni, P. (2004). Artificial neural network-based techniques for the retrieval of SWE and snow depth from SSM/I data, *Remote Sens. .Environ.*, **90** (1), 76-85.

14. Bacour, C., Baret, F., Béal, D., Weiss, M., Pavageau, K. (2006). Neural network estimation of LAI, fAPAR, fCover and LAI×Cab, from top of canopy MERIS reflectance data: Principles and validation, *Remote Sens. .Environ.*, **105**(4), 313-325.

15. Verger, A., Baret, F., Weiss, M. (2008). Performances of neural networks for deriving LAI estimates from existing CYCLOPES and MODIS products. *Remote Sens. .Environ.*, 112(6), 2789-2803.

16. Vilas-González, L., Spyrakos, E., Torres-Palenzuela, J. M. (2011). Neural network estimation of chlorophyll a from MERIS full resolution data for the coastal waters of Galician rias (NW Spain), *Remote Sens. .Environ.*, **115**(2), 524-535.

17. Picchiani, M., Del Frate, F., Piscini, A., Chini, M., Corradini, S., Merucci, L., Stramondo, S, (2012). Associative memory techniques for the exploitation of remote sensing data in the monitoring of volcanic events. In Proceedings of International Geoscience and Remote Sensing Symposium IGARSS '12.

18. Schlüssel, P., T. H. Hultberg, P. L. Phillips, T. August, and X. Calbet (2005). The operational IASI level 2 processor. *Advances in Space Research* **36**, 982–988, doi:10.1016/j. Asr.2005.03.008.

19. Blumstein, D., Chalon, G., Carlier, T., Buil, C., Hebert, P., Maciaszek, T., Ponce, G., Phulpin, T., Tournier, B., Simeoni, D., Astruc, P., Clauss, A., Kayal, G., and Jegou, R. (2004). IASI Instrument: Technical overview and measured performances. In Proceedings of SPIE, 5543, 196–207.

20. Clerbaux, C., Boynard, A., Clarisse, L., George, M., Hadji-Lazaro, J., Herbin, H., Hurtmans, D., Pommier, M., Razavi, A., Turquety, S., Wespes, C., and Coheur, P.-F. (2009). Monitoring of atmospheric composition using the thermal infrared IASI/MetOp sounder, *Atmos.. Chem. Phys.*, **9**, 6041–6054, doi:10.5194/acp-9-6041-2009.

21. Rodgers, C. D. (2000). *Inverse Methods for Atmospheric Sounding: Theory and Practice*, World Scientific, River Edge, NJ, USA.

22. Saunders, R. W., Matricardi, M., and Brunel, P. (1999). An improved fast radiative transfer model for assimilation of satellite radiance observations, *Q. J. Roy. Meteor. Soc.*, **125**, 1407–1425.

23. Rosenblatt, R. (1962). *Principles of Neurodynamics*, Spartan Books, New York.

24. Hecht-Nielsen, R. (1990). *Neurocomputing*, Addison-Wesley, Reading, MA.

25. Bishop, C. (1995). *Neural Networks For Pattern Recognition*, Oxford University Press, Oxford.

26. Rumelhart, D.E., Hinton, G.E., Williams, R.J. (1986). Learning internal representation by error propagation. In: Rumelhart, D.E., McClleland, J.L. (Eds.). Parallel Distributed Processing: Exploration in the Microstructure of Cognition, Vol. 1. MIT Press, Cambridge, MA, Chapter 8.

27. Haykin, S. (1999). *Neural Networks A Comprehensive Foundation* (second ed) Prentice-Hall, NJ, USA.

28. Hassoun, M.H. (1995). *Fundamentals of Artificial Neural Networks*, MIT Press, Cambridge, MA.

29. Prechelt, L. (1998). Automatic Early Stopping Using Cross Validation: Quantifying the Criteria. *Neural Networks*, **11**(4), 761-767.